**NUEJ**
**Naresuan University Engineering Journal**

# Low Frequency Planar Wireless Power Transfer with Impedance Matching using L-Section Matching Network for Underwater EVs

Hajira Masood, Watchara Amasiri, Artit Rittiplang, and Wanchai Pijitrojana*

Department of Electrical and Computer Engineering, Thammasat School of Engineering, Thammasat University, Pathum Thani, Thailand 12120

*Corresponding author e-mail: pwanchai@engr.tu.ac.th

(Received: 14 August 2022, Revised: 24 June 2023, Accepted: 26 June 2023)

**Abstract**

For the Wireless Power Transfer (WPT) system, the impedance Matching (IM) is the technique in which a wide range of resonant and strong coupling structures have been studied which mostly operate at an ideal parameter, i.e., resistive load and high RF greater than1MHz, however these parameters have some limitations in which the most important is that the high frequency is usually inefficient and complex load. This paper presents an L-section matching network to find the ideal load and source conditions. Thus, under the normal load and source conditions, we estimate the maximum power transfer efficiency and describe how to configure the matching network for the given load and source conditions for low-frequency WPT system. The L-section matching network to connect to a WPT structure using air-core spiral coils. The following configuration of network can operate at a low frequency of 20 kHz. From the calculation the moderate efficiency is 67 % while the efficiency from the experiment is 60 % at 9-cm transfer distance without an ideal parameter. The applications of the proposed work are suitable for underwater electric vehicles. Since the eddy current loss of seawater is critical when the operating frequency is higher than 250 kHz.

**Keywords:** impedance matching, Low-frequency wireless power transfer, L-section matching network, wireless power transfer system for underwater electric vehicles.

## 1. INTRODUCTION

Wireless power transfer based on magnetic resonant coupling appears to be difficult for commercial applications until the last few years (Shinohara et al., 2017, Li et al., 2015). Nowadays the common form of WPT mainly consists of three ways, radio waves or microwaves, inductive coupling or inductive power transmission and electromagnetic resonant coupling. It has been widely used in many applications as highlighted in Fig.1.

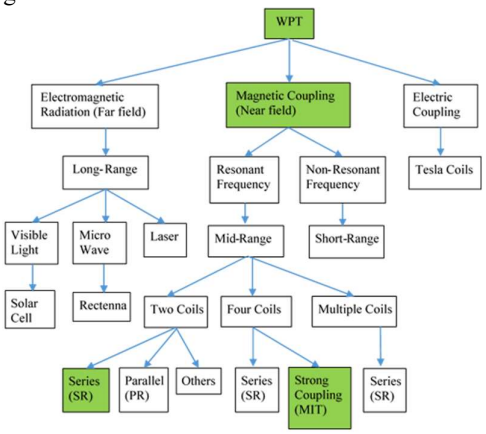


**Figure 1** WPT categories and structures (Jang et al., 2016).

For an efficient power transmission, WPT should fulfill three conditions: (a) high power, (b) large air gap, and (c) high efficiency (Li et al., 2015). The efficiency of WPT system also depends on WPT techniques. Transfer efficiencies of different WPT techniques for both near and far region, 70 % to 90 % transfer efficiency can be achieved through inductive coupling while magnetic resonance coupling offers a moderate efficiency of 40% to 60%. These transfer efficiencies decay with distance. Especially, in the underwater environment, WPT technology solves the problem of wet plugging and the unplugging of underwater energy supply and provides a safer method for the rapid charging of autonomous underwater vehicles (AUVs) (Zhang et al., 2016, Yan et al., 2019, Kim et al., 2019, Dou et al., 2019) and unmanned underwater vehicles (UUVs). Therefore, in view of the widespread application of underwater WPT technology, it is of great research significance to improve its energy transmission efficiency.

The WPT system in the air uses one or more pairs of induction coils. The alternating current (AC) of the primary-side coil generates the induced alternating current (AC) in the coupled secondary-side coil, and then the direct current (DC) is generated through rectification to complete the power supply to the equipment. The process of underwater WPT is similar to that in the air, but the medium in the transmission area changes from air

to seawater. There are various challenges for underwater WPT summarized here. 1. What is the effect of high conducting water medium on electrical parameters of WPT system? 2. How coil radiation resistance is affected by seawater? 3. What are the main losses incurred and how to minimize these losses? 4. If any loss is highly dependent of frequency then how to select an operating frequency to achieve an efficient wireless power transmission (Syed et al., 2020)

Therefore, the underwater WPT process considered in this paper is to solve the third and fourth challenges. Since for underwater, the coupling characteristics between the coils have changed, and the changed magnetic field will generate eddy current in the seawater, which brings new energy loss, namely, eddy current loss. From (Shi et al., 2014), they analyzed various losses in underwater WPT systems, including copper loss, semiconductor loss, core loss, and eddy current loss by using circuit analysis and electromagnetic field (EMF) simulation.

In this paper, we focused to reduce eddy current loss. In order to reduce the eddy current loss of underwater WPT systems, several researchers have studied it. From (Zhang et al., 2018), they analyzed some factors that affect the eddy current loss of underwater charging systems, and used EMF simulation software to optimize the number of coils turns on the primary side and the secondary side and the frequency of the AC source, thereby reducing the eddy current loss, and also designed experiments to verify optimization results. From (Zhang et al., 2019), they presented a new coil structure, taking advantage of two primary-side coils placed symmetrically adjacent to each side of the secondary-side coil to reduce the eddy current loss of WPT systems for underwater vehicles.

Seawater medium is a good electromagnetic conductor. At a low electromagnetic frequency, since it satisfies the loss tangent, $\sigma/(\omega \cdot \varepsilon) >> 1$. The expressions for the seawater attenuation constant and phase constant can be simplified as follows: $\alpha \approx \beta \approx \sqrt{f\pi\mu\sigma} = 0.004\sqrt{f}$. The attenuation constant is not only related to the conductivity, permeability and dielectric constant of the seawater medium, but also closely related to the frequency of the electromagnetic wave. The attenuation is positively correlated with frequency, and this is more obvious in the high-frequency range. Therefore, it is given that the eddy current loss is caused by electromagnetic wave transmission in seawater medium, it can be reduced by controlling the transmission frequency to achieve efficient energy transmission.

A remarkable innovation of non-radiated wireless power transfer (WPT) system using strongly magnetic resonant coupling has been observed in recent years, and due to its operating range and efficiency, it has shown more prospects for powering devices (Shinohara et al., 2017, Jang et al., 2016, Choi et al., 2015, Li et al., 2016). Because the magnetic field weakly interacts with other objects in the surrounding environment, the resonant circuits are used to improve the efficiency (Shinohara et al., 2017). Nowadays, most of the WPT structures are usually presented the two-coil Series Resonance (SR) and strong coupling (MIT team) models as shown in Fig. 2 (a) - (b) (Shinohara et al., 2017, Jang et al., 2016, Choi et al., 2015, Li et al., 2016, Zhang et al., 2016, Yan et al., 2019, Kim et al., 2019). These structures can be achieved the high transfer distance at high frequency as shown in Fig. 2 (c), the transfer distance of 56 cm is achieved at 5.26 MHz with 36 % efficiency.

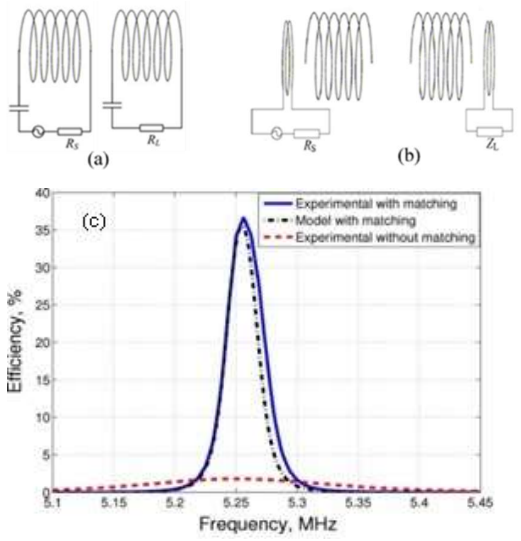


**Figure 2** (a) The two-coil SR structure (Zhang et al., 2014c). (b) The strong coupling structure (Zhang, et al., 2014b) (c) The two-coil SR structure of the ten-tum at the transfer distance of 56 cm shows the high efficiency at about 5.26 MHz (Yan et al., 2019).

The Impedance Matching (IM) condition in Fig. 2 (a) - (b) is achieved by using an optimal parameter (usually either load or transfer distance) for improving the efficiency. However, an optimal parameter is a fixed value that limits the design, so this issue can be solved by using L-section matching networks as shown in Fig. 3.

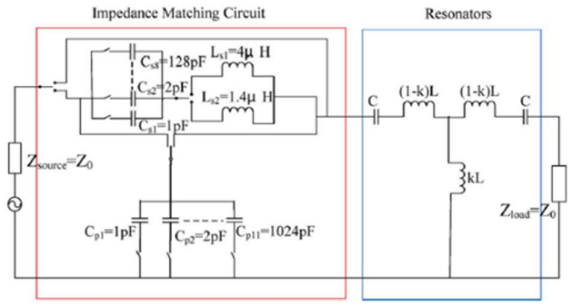


**Figure 3** The IM circuit is connected to the two-coil SR structure at 13.56 MHz frequency operation (Beh et al., 2013).

As shown in Fig. 3, they proposed the high frequency operation at 13.56 MHz for obtaining the high transfer distance and efficiency. Unfortunately, the high - frequency RF sources are usually inefficient (Zhang et al.,

2014, Zhang et al., 2014, Zhang et al., 2014), and the high-frequency operation causes eddy current loss for underwater media, electromagnetic interference, tissue absorption, etc. (Hui et al., 2014, Zhang et al., 2014, Zhang et al., 2014, Zhang et al., 2014, Jolani et al., 2014).

From (Wang et al., 2022), the simulation results of a single-plane coil using electromagnetic field simulation software are shown in the Fig. 4 - 6. Fig. 7 shows the AC resistance and eddy current loss resistance of the planar coil in the air and seawater, respectively. Fig. 8 and 9 show the comparison of its electric field intensity modulus and phase angle under different frequency excitations. It can be seen from the results as shown in the figures below that in the air medium, the eddy current loss resistance is always zero, while in the seawater medium, with the increase in frequency, the eddy current loss resistance increases rapidly. However, with the low frequency under 100 kHz, the eddy current loss resistance, the electric field intensity modulus and phase angle under different frequency excitations do not affect the underwater WPT system.

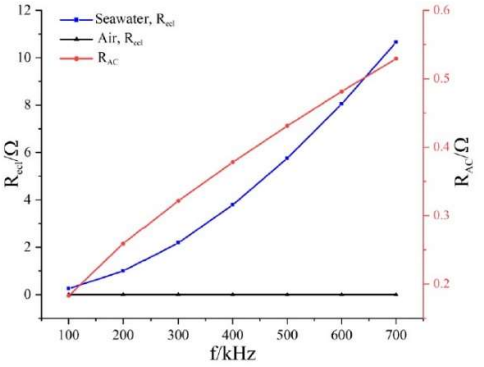


**Figure 4** Variation of AC resistance and eddy current loss resistance with frequency.

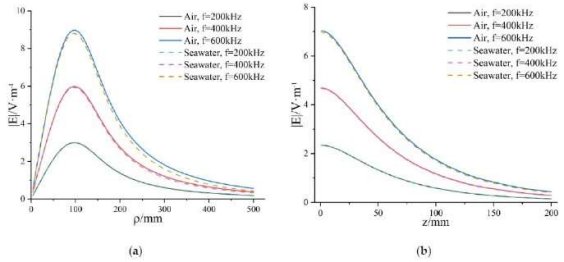


**Figure 5** Modulus of electric field intensity generated by planar coil in the (a) radial direction (b) axial direction.

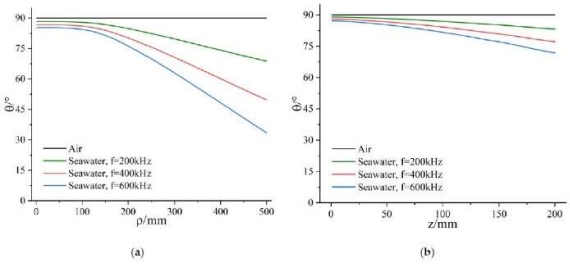


**Figure 6** Phase of electric field intensity generated by planar coil in (a) radial direction (b) axial direction.

Thus, in this work, we propose a low-frequency WPT by a secondary capacitor (C2) to parallel to the secondary coil as shown in Fig. 4, because of the high-quality factor (QParallel = RL/ωL2) at a low-frequency operation (Ahn et al., 2015). And spiral circular coils are applied for a planar WPT. The result of the L-section circuit is used in this WPT because its resistive losses are less than the resistive losses of π- and T-section circuits (Pozar et al., 2012). Finally, we also show the resistive losses of two coils in the equivalent circuit because these values are the important factors which determine the efficiency of the WPT.

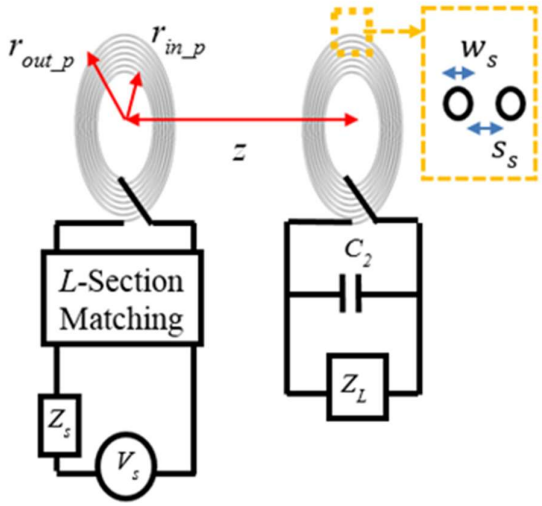


**Figure 7** The proposed structure.

## 2. ELECTRICAL PARAMETERS

To start the design of the proposed structure, the electrical parameters of the two-coil side in Fig. 7 must be calculated. Let $r_{out}$, $r_{in}$, $w$, $s$, $z$, and N are the outer radius of the coil, the inner radius of the coil, a diameter of the conductor, line separation, transfer distance, and a number of turns. The equivalent circuit of Fig. 7 can be shown in Fig. 8. $Z_L$ is a complex load ($R_L + jX_L$).

The resistances ($R_1$ and $R_2$), the mutual inductance ($M$), the self-inductance ($L_1$ and $L_2$), and the secondary capacitance ($C_2$) are described below.

1. $R_1$ and $R_2$ can be calculated from Eq. (1) (Hui et al., 2014)

$$R_{1,2} = \frac{\rho l}{\pi (w/2)^2} \frac{w}{2\delta \left(1 - e^{-\frac{w}{\delta}}\right)} \quad (1)$$

Where $\delta$ is the skin depth, $\delta = \sqrt{(\rho/\pi\mu_0 f)}$, $\rho$ is the resistivity of copper ($1.68\times10^{-8}$ Ω.m), $\mu_0$ is the free space permeability constant ($4\pi\times10^{-7}$ H·m$^{-1}$), and $l$ is the length of the conductor, $l = \pi N(2r_{in} + wN - w)$.

2. $M$ can be calculated as shown below. (Raju et al., 2014)

$$M = \left(\frac{4}{\pi}\right)^2 \sum_{i=1}^{i=N_p} \sum_{j=1}^{j=N_s} M_{ij} \qquad (2)$$

Where $N_p$ is number of primary turns and $N_s$ is number of secondary turns;

$$M_{ij} = \frac{\mu_0 \pi a_i^2 b_j^2}{2\left(a_i^2 + b_j^2 + z^2\right)^{\frac{3}{2}}} \cdots \left(1 + \frac{15}{32}\gamma_{ij}^2 + \frac{315}{1024}\gamma_{ij}^4 + \frac{15015}{65536}\gamma_{ij}^6\right) \qquad (3)$$

$$a_i = r_{out\_p} - (i-1)\left(w_p + s_p\right) - \frac{w_p}{2} \qquad (4)$$

$$b_j = r_{out\_s} - (j-1)(w_s + s_s) - \frac{w_s}{2} \qquad (5)$$

$$\gamma_{ij} = \frac{2a_i b_j}{a_i^2 + b_j^2 + z^2} \qquad (6)$$

3. $L_1$ and $L_2$ are obtained as shown in Eq. (7). (Mohan et al., 1999)

$$L = \frac{\mu_0 N^2 (r_{out} + r_{in})}{2}\left[\ln\left(\frac{2.46}{\varphi}\right) + 0.2\varphi^2\right] \qquad (7)$$

$$\varphi = \frac{r_{out} - r_{in}}{r_{out} + r_{in}} \qquad (8)$$

4. $C_2$ is calculated as shown in Eq. (9) to maximize the load voltage.

$$C_2 = \frac{1}{L_2 \omega^2} \qquad (9)$$

The electrical parameters as stated above are used to calculate the reflected impedance $Z_P$ as shown in Eq. (10).

$$Z_P = \alpha + j\beta \qquad (10)$$

Where,

$$\alpha = R_1 + \frac{\omega^2 M^2 (R_2 + Y)}{A} \qquad (11)$$

$$\beta = \omega L_1 - \left[\frac{\omega^2 M^2}{A} \cdots \frac{\left(\omega L_2 - \omega C_2 R_L Y + \frac{(X_L - \omega C_2 X_L^2)Y}{R_L}\right)}{A}\right] \qquad (12)$$

$$A = (R_2 + Y)^2 + \cdots \left(\omega L_2 - \omega C_2 R_L Y + \frac{(X_L - \omega C_2 X_L^2)Y}{R_L}\right)^2 \qquad (13)$$

$$Y = \frac{R_L}{(1 - \omega C_2 X_L)^2 + \omega^2 C_2^2 R_L^2} \qquad (14)$$

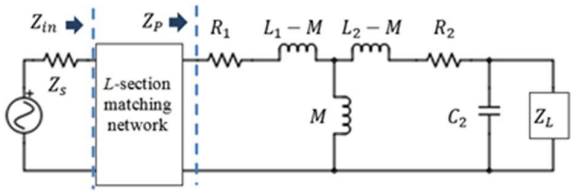


**Figure 8** The equivalent circuit of the proposed structure.

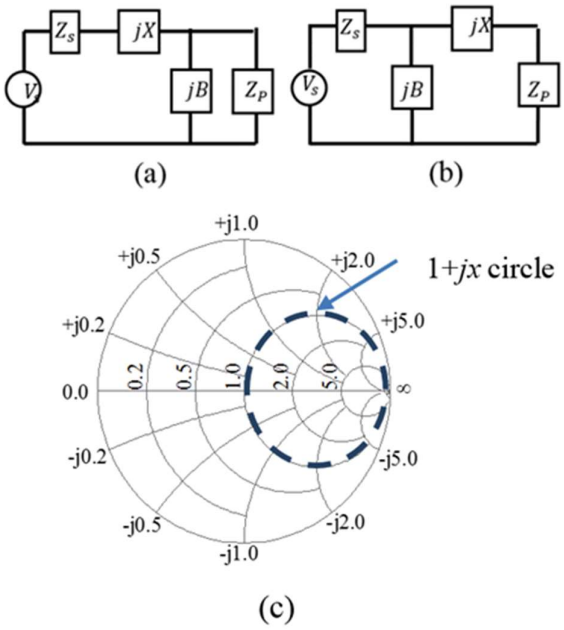


**Figure 9** The two possible *L*-section matching circuits (a) Network $Z_p/Z_s$ inside the 1+*j*x circle. (b) Network for $Z_p/Z_s$ outside the 1+*j*x circle. (c) The impedance 1+*j*x circle on the Smith chart.

## 3. THEORY

From Fig. 8, the IM condition ($Z_s^*$- $Z_{in}$ = 0) is commonly used to maximize the input power. The intrinsic impedance of the RF source is defined as $Z_s$. The circuit of Fig. 8 can be presented as two possible matching circuits as shown in Fig.9(a) and 9(b).

Accordingly, a suitable circuit must be selected and then a reactance $X$ and a susceptance ($B$) for achieving the IM condition are calculated (Zhang et al., 2014). Firstly, we calculate the normalized reflected impedance $z_p$ ($Z_p/Z_s$). If $z_p$ is inside the 1+*jx* circle on the Smith chart of Fig. 9(c), then the circuit of Fig. 9(a) is used.

$$X = \frac{1}{B} + \frac{\beta Z_s}{\alpha} - \frac{Z_s}{B\alpha} \qquad (15)$$

$$B = \frac{\beta \pm \sqrt{\alpha/Z_s}\sqrt{\alpha^2 + \beta^2 - \alpha Z_s}}{\alpha^2 + \beta^2} \qquad (16)$$

Also, if $z_p$ is outside the 1+$jx$ circle on the Smith chart of Fig. 9(c), then the circuit of Fig. 9(b) is used.

$$X = \pm\sqrt{\alpha(Z_s - \alpha)} - \beta \qquad (17)$$

$$B = \pm\frac{1}{Z_s}\sqrt{(Z_s - \alpha)/\alpha} \qquad (18)$$

From Eq. (15) to (18), a positive $X$ implies an inductor and a negative $X$ implies a capacitor, while a positive $B$ implies a capacitor and a negative $B$ implies an inductor (Pozar et al., 2012).

To demonstrate the design processes clearly, the design is summarized as the flowchart as show in Fig. 10.

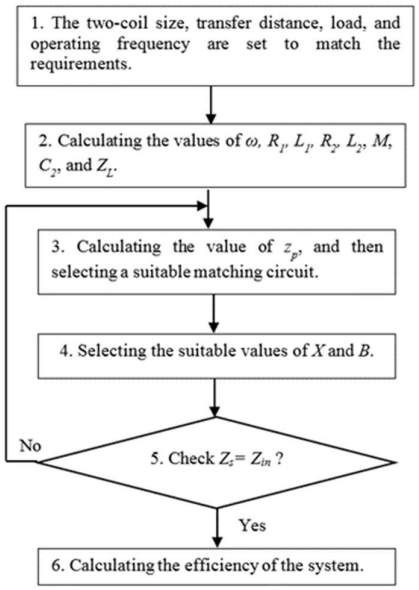


**Figure 10** Flowchart of design.

## 4. Calculation and Experiment

In this section, the physical parameters as shown in Fig. 7 are required as follows: $z$ = 9 cm, $r_{out\_p} = r_{out\_s}$ = 8 cm, $r_{in\_p} = r_{in\_s}$ = 6.5 cm, $w_p = w_s$ = 1 mm, $s_p = s_s$ = 0.2 mm, and $N_p = N_s$ = 10 turns. The RF source voltage is set to be 20 V with the intrinsic impedance $Z_s$ = 50 Ω, and the operating frequency is set to be 20 kHz because the RF source is efficient. A load is assumed to be 25 Ω. The calculated electrical parameters using Eq. (1) - (10) are shown in Table 1.

The normalized reflected impedance $z_p$ is outside the 1+$jx$ circle on the Smith chart, so the circuit of Fig. 9(b) is used. Then, from Eq. (17) two reactances $X$ are calculated as 1.8051 Ω and -8.9521 Ω, while two susceptances $B$ are calculated as 0.1837 $\Omega^{-1}$ and - 0.1837 $\Omega^{-1}$ by using Eq. (18). Next, the system has two matching circuits as shown in Fig.11(a) and 11(b), where the parameters of Fig.11(a)-11(b) are shown in table 2.

**Table 1** The electrical parameters

| Parameter | Value |
|---|---|
| $L_1 = L_2$ (μH) | 28.89 |
| $R_1 = R_2$ (Ω) | 0.11 |
| $M$ (μH) | 4.3733 |
| $C_2$ (μF) | 2.192 |
| $Z_p$ (Ω) | 0.5854+$j$3.5735 |
| $z_p = Z_p / Z_s$ (Ω) | 0.0117+$j$0.0715 |

**Table 2** Parameters of the matching circuits

| Parameter | Value |
|---|---|
| $L_s$ (μH) | 14.365 |
| $C_p$ (μF) | 1.4622 |
| $L_p$ (μH) | 43.309 |
| $C_s$ (μF) | 0.89 |

From Fig. 11(c), solution 1 is required to connect to the system because its bandwidth is significantly better than of the solution 2 (Pozar et al., 2012, Raju et al., 2014). Hence, an equivalent circuit of the design can be illustrated by Fig. 12.

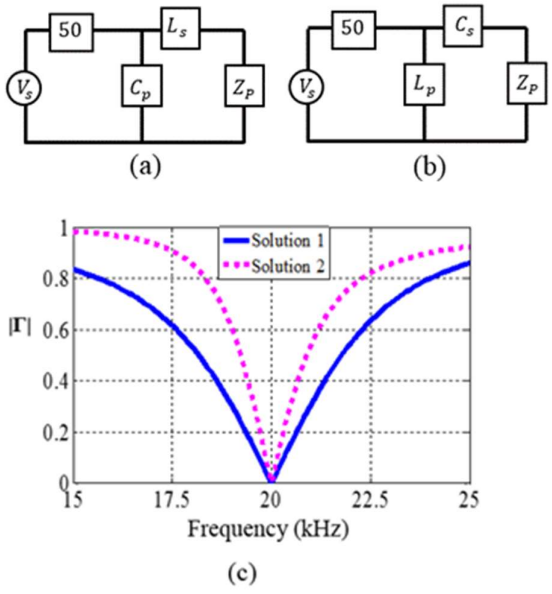


**Figure 11** Two matching circuits: (a) solution 1 (b) solution 2 (c) reflection coefficient magnitude |Γ| versus frequency.

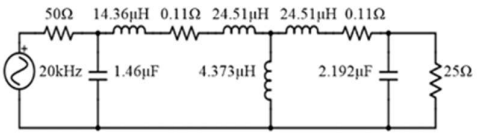


**Figure 12** An equivalent circuit model of the design.

The input impedance $Z_{in}$ of the system is calculated as 50.02 Ω using (19) so that the system achieves the IM condition. Then *Z*- and *ABCD*-parameter matrices as shown in Eq. (20) - (21) are used.

$$Z_{in} = Z_{11} - \frac{Z_{12}Z_{21}}{Z_{22} + Z_L} \qquad (19)$$

Where,

$$\begin{bmatrix} Z_{11} & Z_{12} \\ Z_{21} & Z_{22} \end{bmatrix} = \begin{bmatrix} \frac{A_a}{C_c} & \frac{A_a D_d - B_b C_c}{C_c} \\ \frac{1}{C_c} & \frac{D_d}{C_c} \end{bmatrix} \qquad (20)$$

$$\begin{bmatrix} A_a & B_b \\ C_c & D_d \end{bmatrix} = \begin{bmatrix} 1 & j\omega L_p \\ j\omega C_s & 1 - \omega^2 L_p C_s \end{bmatrix} \cdots$$

$$\cdots \begin{bmatrix} 1 & R_1 + j\omega L_1 \\ 0 & 1 \end{bmatrix} \begin{bmatrix} 0 & -j\omega M \\ \frac{-j}{\omega M} & 0 \end{bmatrix} \cdots$$

$$\cdots \begin{bmatrix} 1 & R_2 + j\omega L_2 \\ 0 & 1 \end{bmatrix} \begin{bmatrix} 1 & 0 \\ j\omega C_2 & 1 \end{bmatrix} \qquad (21)$$

The efficiency of the system can be calculated as 67 % by using Eq. (22) (Pozar et al., 2005).

$$\eta = \frac{Re\{Z_L\}}{Re\{Z_{in}\}} \left| \frac{Z_{21}}{Z_{22} + Z_L} \right|^2 * 100 \qquad (22)$$

An experiment is conducted and set up according to the circuit in Fig. 12, which is illustrated in Fig. 13.

**Table 3** Current, voltage signal and efficiency

| | $I_{in}$ (A) | $Z_{in}$ (Ω) | $V_L$ (V) | $\eta$ (%) |
|---|---|---|---|---|
| Calculation | 0.4∠0° | 50∠0° | 11.244∠-83° | 67 |
| Experiment | 0.41∠-3° | 48.78∠3° | 10.1∠-71° | 60 |

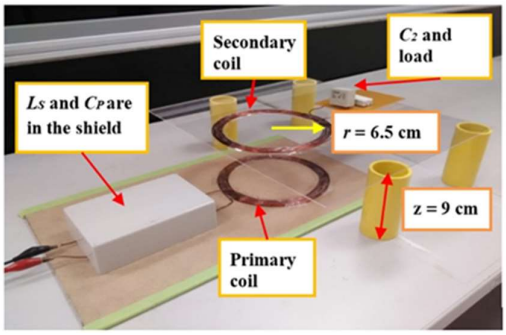


**Figure 13** Experimental setups with C2 ≈ 2.2 µF, ZL = 25 Ω, as well as CP ≈ 1.5 µF and LS ≈ 15 µH in the shield chassis, and η = 60 %.

The input current and load voltage signals of the experiment are measured as shown in Table 3 and Fig. 14.

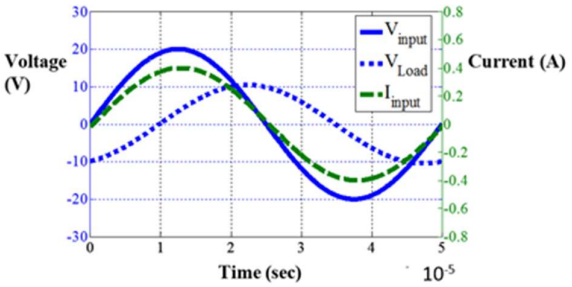


**Figure 14** The measured Iin, Vin, and VL from the experiment.

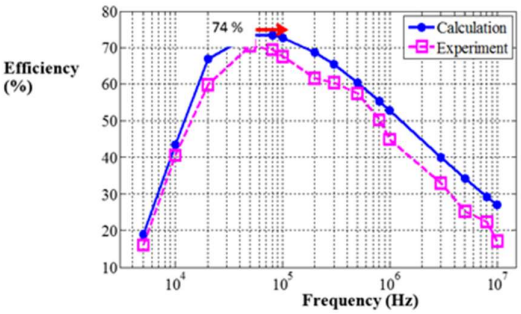


**Figure 15** The efficiency of the system versus the frequency.

Fig. 15 shows a 3° phase shift between the input current and voltage, and the input impedance $Z_{in}$ is equal to 48.78∠3° Ω. The experiment is approximately closed to the IM condition. This is due to the parasitic losses of the circuit and devices. Furthermore, the system is also conducted by varying the frequencies in the range from 5 kHz to 10 MHz, while also maintain the IM condition as shown in Fig. 12. The maximum efficiency is equal to 74 % at the frequency of 50 kHz.

From the results and the circuit of Fig. 12, the proposed structure can operate at low frequencies which are less than the critical frequency of 250 kHz for underwater WPT system, while maintaining high efficiency (the maximum efficiency is 74 % at 50 kHz) without an optimal parameter. However, the transfer distance is in the short range of 9 cm so that it is easy to control the magnetic flux along the transfer distance.

## 5. Conclusion

Most of the WPT structures proposed are the SR structure and the strong coupling structures under the IM condition using an optimal parameter, but an optimal parameter (fixed value) limits the design. In addition, they operate at a high frequency of several MHz to GHz. Unfortunately, the high-frequency RF sources are usually inefficient and difficult to implement, and the high-

frequency operation is well-known to cause several problems, especially for the underwater WPT system. Therefore, to obtain low-frequency operation is the main goal of this paper while it is still maintaining the high efficiency and under the IM condition without an optimal parameter. To compare to the standard design approach, the efficiency of the matching networks designed by using the implemented approach is observed that the significant improvements for efficiency are possible. These improvements are validated by extensive simulations and experiment. Lastly, in this paper, we show that the proposed structure can operate at a low frequency under the IM condition using *L*-section matching with high efficiency using parallel $C_2$. In addition, the planar coils are a more effective candidate for a low-profile and small-footprint WPT system, especially the underwater WPT system.

## 6. ACKNOWLEDGMENT

This work was supported financially by the Master Scholarship from Thammasat School of Engineering, Thammasat University and the Ph.D. Scholarship from Thammasat University, The authors would like to thank the Quantum Technology and Energy Research Group, Thammasat University, for the technical supports.

## 7. REFERENCES

Ahn, D. and Hong, S. (2015). Wireless Power Transfer Resonance Coupling Amplification by Load-Modulation Switching Controller. *IEEE Transactions on Industrial Electronics, 62*(2), 898 - 909. https://doi.org/10.1109/TIE.2014.2336627

Beh T. C., Kato M., Imura T., Oh S., and Hori Y. (2013).Automated Impedance Matching System for Robust Wireless Power Transfer via Magnetic Resonance Coupling. *IEEE Transactions on Industrial Electronics*, 60(9), 3689-3698. https://doi.org/10.1109/TIE.2012.2206337

Choi S. Y., Gu B. W., Jeong S. Y., and Rim C. T. (2015). Advances in Wireless Power Transfer Systems for Roadway Powered Electric Vehicles. IEEE J. Emerg. Sel. *Topics Power Electron*., 3(1), 18 - 36. https://doi.org/10.1109/JESTPE.2014.2343674

Dou, Y., Zhao, D., Ouyang, Z., and Andersen, M.A.E. (2019). Investigation and Design of Wireless Power Transfer System for Autonomous Underwater Vehicle. *In Proceedings of the 2019 IEEE Applied Power Electronics Conference and Exposition (APEC)*, 17(2), 3144–3150. https://doi.org/10.1109/APEC.2019.8721879

Fu M., Zhang T., Zhu X., and Ma C. (2013). A 13.56 MHz wireless power transfer system without impedance matching networks. Proc. *WPTC*, 222–225. https://doi.org/10.1109/WPT.2013.6556923

Han Y., and Perreault D. J. (2006). Analysis and Design of High Efficiency Matching Networks. *IEEE Transactions on Power Electronics,* 21(5),484-1491. https://doi.org/10.1109/TPEL.2006.882083

Hui, S. Y. R. Zhong, W. and Lee, C. K. (2014). A Critical Review of Recent Progress in Mid-Range Wireless Power Transfer. *IEEE Transactions on Power Electronics*, 29(9),4500-4511. http://dx.doi.org/10.1109/TPEL.2013.2249670

Jang Y. J., Suh E. S., and Kim J. W. (2016). System Architecture and Mathematical Models of Electric Transit Bus System Utilizing Wireless Power Transfer Technology. *IEEE Syst. J*., 10(2), 495-506. https://doi.org/10.1109/JSYST.2014.2369485

Jolani, F. Yu, Y. and Chen, Z. (2014). A Planar Magnetically Coupled Resonant Wireless Power Transfer System Using Printed Spiral Coils. *IEEE Antennas and Wireless Propagation Letters*, 13, 1648-1651. https://doi.org/10.1109/LAWP.2014.2349481

Kim, J., Kim, K., Kim, H., Kim, D., Park, J., and Ahn, S. (2019). An Efficient Modeling for Underwater Wireless Power Transfer Using Z-Parameters. IEEE Trans. *Electromagn. Compat*, 61, 2006–2014. http://dx.doi.org/10.1109/TEMC.2019.2952320

Kumar Ashish, Sinha Sreyam, Sepahvand Alihossein. And Afridi Khurram K. (2018). Improved Design Optimization for High-Efficiency Matching Networks. *IEEE Transactions on Power Electronics*, 33(1). https://doi.org/10.1109/TPEL.2017.2670640

Li S., and Mi C. C. (2015). Wireless power transfer for electric vehicle applications. IEEE J. Emerg. Sel. *Topics Power Electron*., 3(3), 4-17. https://doi.org/10.1109/JESTPE.2014.2319453

Lum Kin Yun, Lindén Maria, and Tan Tian Swee (2015). Impedance Matching Wireless Power Transmission System for Biomedical Device. Stud. *Health Technol. Inform*., 211,225-32. http://dx.doi.org/10.3233/978-1-61499-516-6-225

Mohan S. S., Hershenson M. D. M., Boyd S. P., and Lee T. H. (1999). Simple Accurate Expressions for Planar Spiral Inductances. *IEEE Journal of Solid-State Circuits,* 34(10),1419-1424. https://doi.org/10.1109/4.792620

Pozar, D. M. (2012). 4th Editor, Microwave Engineering. New Jersey. John Wiley and Sons, Inc. Raju S. Wu,

R. Chan M. and Yue C. P. (2014). Modeling of Mutual Coupling Between Planar Inductors in Wireless Power Applications.*IEEE Transactions on Power Electronics*, 29(1), 481-490. https://doi.org/10.1109/TPEL.2013.2253334

Ramrakhyani A.K., Mirabbasi S., and Chiao, M. (2011). Design and Optimization of Resonance-Based Efficient Wireless Power Delivery Systems for Biomedical Implants. *IEEE Transactions on Biomedical Circuits and Systems*, 5(1), 48-63. https://doi.org/10.1109/tbcas.2010.2072782

Shi, J., Li, D., and Yang, C. (2014). Design and Analysis of an Underwater Inductive Coupling Power Transfer System for Autonomous Underwater Vehicle Docking Applications. *J. Zhejiang Univ.Sci.* C 15, 51–62. https://doi.org/10.1631/jzus.C1300171

Shinohara, Naoki & Mitani, Tomohiko (2017). Impedance Matching in Wireless Power Transfer. *IEEE Transactions on Microwave Theory and Techniques*, 65(2), 1-9. https://doi.org/10.1109/TMTT.2016.2618921

Syed Agha Hassnain Mohsan, Mushtag Ali Khan, Laraba Selsabil Rokia, Asad Islam, Arfan Mahmood, and Alireza Mazinani (2020). A Review on Research Challenges, Limitations and Practical Solutions for Underwater Wireless Power Transfer. *International Journal of Advanced Computer Science and Applications 11*(8). https://doi.org/10.14569/IJACSA.2020.0110869

Thomas, E. M. Heebl, J. D. Pfeiffer, C. and Grbic, A. (2012). A Power Link Study of Wireless Non-Radiative Power Transfer Systems Using Resonant Shielded Loops. *IEEE Transactions on Circuits and Systems I: Regular Papers*, 59(9), 2125-2136. https://doi.org/10.1109/TCSI.2012.2185295

Urano, Mitsuhiro, and Akira Takahashi (2016). Study on underwater wireless power transfer via electric coupling. *2016 IEEE International Meeting for Future of Electron Devices*, Kansai (IMFEDK). https://doi.org/10.1109/IMFEDK.2016.7521674

Wang Jiale, Song Baowei, and Wang Yushan (2022). A Method to Reduce Eddy Current Loss of Underwater Wireless Power Transmission by Current Control. *Appl. Sci. 2022*, 12(5), 2435. https://doi.org/10.3390/app12052435

Yong Huang, Naoki Shinohara, and Tomohiko Mitani (2017). Impedance Matching in Wireless Power Transfer. *IEEE TRANSACTIONS ON MICROWAVE THEORY AND TECHNIQUES*, 65(2) https://doi.org/10.1109/TMTT.2016.2618921

Yan, Z., Song, B., Zhang, Y., Zhang, K., Mao, Z., and Hu,Y. A. (2019). A Rotation-Free Wireless Power Transfer System with Stable Output Power and Efficiency for Autonomous Underwater Vehicles. IEEE Trans. *Power Electron.* 2019, 34,4005–4008. https://doi.org/10.1109/TPEL.2018.2871316

Zhang, K.-H., Zhu, Z.-B., Song, B.-W.; Xu, D.-M. (2016). A Power Distribution Model of Magnetic Resonance WPT System in Seawater. *Proceedings of the 2016 IEEE 2nd Annual Southern Power Electronics Conference (SPEC),*1–4. https://doi.org/10.1109/SPEC.2016.7845532

Zhang, K.-H., Zhu, Z.-B., Du, L.-N., and Song, B.-W. (2018). Eddy Loss Analysis and Parameter Optimization of the WPT System in Seawater. J. *Power Electron*., 18, pp. 778–788. http://dx.doi.org/10.6113/JPE.2018.18.3.778

Zhang, K., Zhang, X., Zhu, Z., Yan, Z., Song, B., and Mi, C.C. (2019). A New Coil Structure to Reduce Eddy Current Loss of WPT Systems for Underwater Vehicles. *IEEE Trans. Veh. Technol*., 68, 245–253. https://doi.org/10.1109/TVT.2018.2883473

Zhang, Y. Zhao, Z. and Chen, K. (2014). Frequency Decrease Analysis of Resonant Wireless Power Transfer. *IEEE Transactions on Power Electronics*, 29(3), 1058–1063. https://doi.org/10.1109/TPEL.2013.2277783

Zhang, Y. Zhao, Z. and Chen, K. (2014). Frequency Splitting Analysis of Four-Coil Resonant Wireless Power Transfer. *IEEE Transactions on Industry Applications*, 50(4), 2436-2445. https://doi.org/10.1109/TIA.2013.2295007

Zhang, Y. and Zhao, Z. (2014). Frequency Splitting Analysis of Two-Coil Resonant. *IEEE Antennas and Wireless Propagation Letters*, 13, 400-402. https://doi.org/10.1109/LAWP.2014.2307924